Pergamon

Int. J. Solids Structures Vol. 32, No. 20, pp. 3015–3036, 1995

0020-7683/95 $9.50 + .00

0020-7683(94)00261-4

ANALYSIS OF POSTBUCKLING BEHAVIOR OF LINE PIPE SUBJECTED TO COMBINED LOADS

ZHILONG ZHOU and D. W. MURRAY
Department of Civil Engineering, University of Alberta, Edmonton, Alberta T6G 2G7, Canada

(*Received* 29 *July* 1993; *in revised form* 3 *October* 1994)

Abstract—A method is presented to incorporate the local buckling behavior of line pipe, determined from three-dimensional large deformational elastic–plastic shell analysis, into an interactive soil-structure beam model of a pipeline. The finite element model for the analysis of the pipe as a shell is described and the influence on the results of the buckling analysis of various load combinations are examined from the point of view of buckling configurations, moment–curvature curves and cross-sectional deformations. A method of extracting the stiffness properties of the pipe from these analyses is then described and a technique for determining stiffness coefficients from these properties is developed.

1. INTRODUCTION

Pipelines in regions of discontinuous permafrost are subject to combined loads consisting of combinations of internal pressure, axial load and bending moment. Overall, a pipeline behaves as a beam structure. However, the deformations are often large enough to induce strains that are significantly greater than the yield strain. As a result, the pipe wall may buckle locally in elastic–plastic manner. Response of the pipeline can be significantly altered by this local buckling behavior.

A procedure to analyze pipelines for this kind of behavior has been developed by the authors (Zhou and Murray, 1993a, 1995a). This procedure divides the response prediction into two steps. In the first step, a three-dimensional shell model is used to analyze local deformational behavior that includes local buckling, and a set of characteristic cross-sectional stiffness properties are then abstracted from these analyses. In the second step, the effects of the local behavior are integrated into the overall behavior of the line by using the generated cross-sectional stiffness properties for a beam model, and the response of the pipeline is then predicted based on this beam model (Zhou and Murray, 1993b, 1995a).

This paper describes analyses of postbuckling behavior of pipe segments under combined loads. Effects of internal pressure and axial load on the postbuckling response are investigated by analyses of pipe segments under different load combinations. Based on these postbuckling analyses, the characteristic stiffness properties are defined. These are taken as input into the beam model in order to predict response of lines in such a way that the effects of local buckling are properly included (Zhou and Murray, 1993a, 1995a).

The paper first describes the three-dimensional shell model employed. Results of postbuckling analyses and postbuckling behavior are then examined with respect to moment–curvature relationships, buckling modes and cross-sectional deformations. Following this, cross-sectional stiffness properties are introduced and the procedures to generate them from shell analyses are described.

2. SIGNIFICANCE AND SCOPE OF POSTBUCKLING ANALYSIS

Postbuckling analysis refers here to nonlinear incremental analysis which is carried out for deformations well beyond the limit point on load–deflection curves. Postbuckling analysis as an analytical tool has important implications for thin shell structures such as pipelines. For structures subjected to imposed deformation, attainment of the load carrying capacity does not precipitate failure because the structure is not required to carry the associated loads, which are self-limiting. Instead, the imposed deformations are required to be absorbed by the structure. However, the hardening and softening characteristics of the postbuckling

response lead to very different characteristics of localization of the deformation and strain (Zhou and Murray, 1995a), and this, in turn, determines the deformation limit states for this particular type of structure (Zhou and Murray, 1993b and 1993c).

In this study, analysis focuses on the phenomenological effects of loading conditions, and therefore it is confined to one particular pipe geometry with one particular set of material properties. This is believed to be sufficient to explore the fundamental physical phenomena. A pipe with outside diameter of 48 inches (1219 mm) and wall thickness of 0.462 inches (11.7 mm) was chosen for this study because this pipe has D/t ratio of 104 and is susceptible to local buckling. This particular size is that used for the Trans-Alaska Pipeline (Bouwkamp and Stephen, 1973) and it is probably the largest size used for a major oil pipeline. The material properties are represented by a bilinear stress–strain model. Based on the properties of Grade XL65 steel, this model has elastic modulus 29800 ksi (205500 MPa), Poisson ratio of 0.3, yield strength of 63.5 ksi (438 MPa) and strain hardening modulus of 124 ksi (855 MPa).

The loading conditions investigated consist of constant internal pressure, constant axial load and variable bending moment. Three levels of internal pressure were chosen to cover the possible range. They are the pressures producing hoop stresses of 0, 35, and 72% of the yield strength. The latter percentage was the highest ratio allowed in the previous design code for Canadian oil pipelines (Canadian Standard Association, 1990). The axial load is used to simulate the effects of the temperature differential. Its magnitude depends on both the temperature differential and the longitudinal restraint provided by surrounding soil. Four levels of axial load were chosen for the low and middle levels of internal pressure. These are, 0, 10, 20, and 40% of the axial yield load in compression. Five levels of axial load were chosen to combine with the high level of internal pressure. These are at the ratios of 0, 20, and 40% for both compression and tension. The highest ratio corresponds to a temperature differential of approximately 73°C with the pipeline assumed to be fully restrained in the longitudinal direction. The combination of the different levels of pressure and axial load described above gives thirteen specimens which are listed in Table 1. In addition to constant pressure and axial load, bending moment is applied as the active load for all of the specimens.

A specimen designation is assigned to each of the specimen simulations. It is composed of three letters followed by a two-digit number. The first letter is P which identifies this series of specimens as a postbuckling analysis series. The second letter is L, M or H, which represents low, middle and high levels of internal pressure, respectively. The third letter is either C or T, which represents compressive or tensile axial load. The two-digit number is the nondimensionalized axial load expressed as a percentage of the axial yield load. The designations of all thirteen specimens are listed in Table 1.

3. FINITE ELEMENT MODEL

The finite element model described below was used for the three dimensional shell analysis of all pipe segments. The model includes the finite element mesh, and the boundary and loading conditions.

Table 1. Specimen loading and designations†

Axial Load (as a % of F_y)	Internal Pressure (as a % of p_i) $L = 0\%$	$M = 35\%$	$H = 72\%$
−40	PLC40	PMC40	PHC40
−20	PLC20	PMC20	PHC20
−10	PLC10	PMC10	—
0	PLC00	PMC00	PHC00
20	—	—	PHT20
40	—	—	PHT40

† 1. Pipe for specimens = 48″(1219 mm) × 0.462″(11.7 mm) DSAW X65 Grade.
2. p_i = Pressure to produce $\sigma_\theta = \sigma_y$.
3. $F_y = A\sigma_y$.

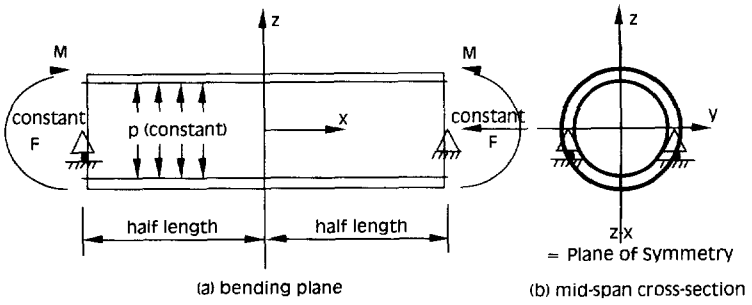

Fig. 1. Loading and boundary conditions, and symmetric planes of pipe segments.

3.1 *Finite element mesh*

The pipe segment under consideration has an outside diameter of 48 inches (1219 mm) and a wall thickness of 0.462 inches (11.7 mm). The length of the pipe segment was chosen as 276 inches (7010 mm) which is about 5.5 times the diameter. The pipe segment is shown in Fig. 1. It is simply supported at both ends and subject to a combination of constant internal pressure, constant axial load and variable moment.

Two symmetry conditions are utilized to reduce the size of the model. These are the symmetry conditions in the bending plane and on the mid-span cross-section, which are in the x–z and y–z planes, respectively, as shown in Fig. 1. The validity of these symmetry conditions will be further discussed in section 3.2. With these symmetry conditions, only a quarter of the pipe segment needs to be discretized. The quarter pipe segment is divided into the main segment and boundary ring with lengths of 132 inches (3353 mm) and 6 inches (152.4 mm), respectively, as shown in Fig. 2. The boundary ring is introduced for simulation of the boundary and loading conditions that are discussed further in the sections to follow. The main segment is discretized by 48 16-node degenerated shell elements and the boundary ring by eighteen 4-node shell elements (Stegmüller, 1984). There are a total of 494 nodes and the mesh is uniform in both the main segment and the boundary ring. The mesh is uniform in the longitudinal direction because the dominant buckle can be anywhere along the segment length in the longitudinal direction. Although buckling usually initiates on the compressive side of the pipe segment, under combination of internal pressure, axial load and bending moment, it develops and expands in the circumferential direction and sometimes covers the entire circumference. Consequently, a uniform mesh is used also in circumferential direction.

The mesh refinement is one of the major considerations. A coarse mesh may not be able to effectively represent the local deformation in the deep postbuckling region. On the other hand, overly refined mesh leads to large systems which require excessive solution time. The particular mesh used here was derived from a series of trials on gradually refined meshes.

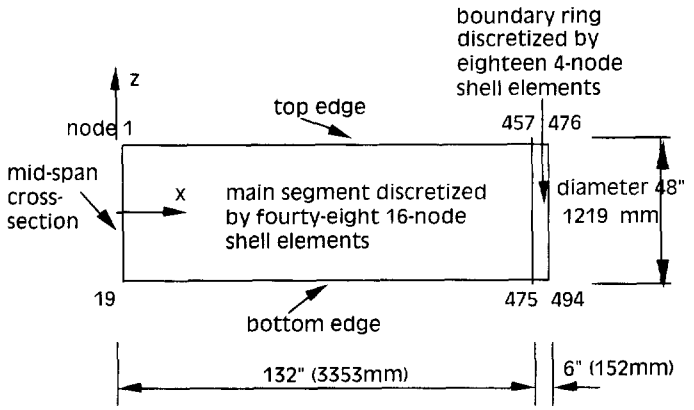

Fig. 2. Global coordinate system and dimensions of the quarter pipe segment.

3.2 *Boundary conditions*

Boundary conditions are needed at the mid-span cross-section, end cross-section, and the top and bottom edges as shown in Fig. 2. The boundary conditions on the mid-span cross-section, and the top and bottom edges are assumed to be the symmetry conditions. The symmetry condition on the bending plane is supported, in general, by the observations from tests (Bouwkamp and Stephen, 1973; Jirsa *et al.*, 1972; Reddy, 1979; Sherman, 1976; Mohareb *et al.*, 1993). The symmetry condition about the mid-span cross-section is more of an assumption than a fact. It is only valid if the buckle occurs in the middle of pipe segment. Nevertheless, because the main objective of postbuckling analysis is to investigate the behavior of a segment which contains a typical buckle, instead of the pipe segment as a whole, it is satisfactory to employ the symmetry condition about the mid-span cross-section provided that either: (a) half a buckle forms at the plane of symmetry; or, (b) an entire buckle is completely contained in the half pipe segment. With the dominant buckle completely simulated somewhere in the half pipe segment, as illustrated in Fig. 3, the loading and deformation characteristics of the buckle can be determined.

Assuming the validity of symmetry conditions as postulated above, the boundary conditions can be detailed as follows. On the top and bottom edges, the symmetry conditions are that the displacements in global y-direction are zero, while the rotation about the global x and z axes are suppressed. The symmetry conditions on the mid-span cross-section are more complicated. Let us first define the local shell coordinate system r, s, t. Axis t represents the direction normal to the shell and axes r and s are in the longitudinal and hoop directions, respectively. The symmetry conditions on the mid-span cross-section are that the displacements in the global x-direction, and the rotations about the t and s axes are suppressed. As shown in Fig. 3 the pipe segment is allowed to shorten or extend as it deforms, and the end cross-section would be allowed to move if the mid-span cross-section were fixed in the x-direction. As an alternative, the mid-span cross-section can be allowed to move in the x-direction while the end cross-section remains fixed in this direction at mid-height. As a result the boundary conditions of displacements on the mid-span cross-section can be modified such that all the nodes on the mid-span cross-section are constrained to have the same displacement in the x-direction. The boundary conditions of rotation remain as stated and can be enforced directly by specifying the boundary codes in the local shell coordinate system.

On the end cross-section, the boundary conditions are that the y-direction displacement at the centroid is suppressed, and the plane of the end section remains plane to simulate the restraint provided by the rest of the pipeline connected to the pipe segment. Rotation

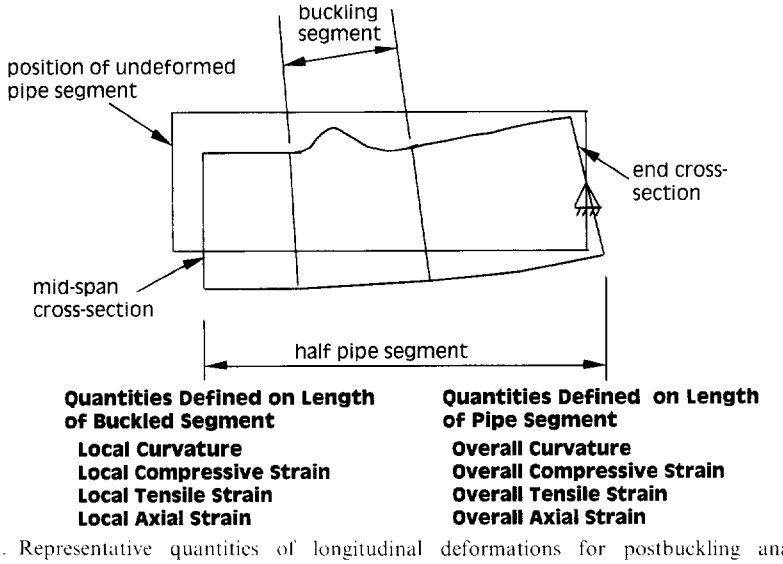

Fig. 3. Representative quantities of longitudinal deformations for postbuckling analysis of pipe segments.

of the end section about the y centroidal axis, and deformation of the section in the plane are permitted.

A boundary ring is used to enforce the boundary conditions on the end cross-section as shown in Fig. 2. The boundary ring is assumed to be elastic and has the same wall thickness as the main segment. The support at the centroidal axis is modelled by supports on the horizontal diameter as shown in Fig. 1(b), and this approximation is acceptable as long as the deformation of the end cross-section is symmetric about its horizontal diameter. Symmetry of the x-displacement about the horizontal diameter on the end section is enforced by coupling the magnitude of the x-direction displacements for the corresponding nodal points on the compression and tension sides. Coupling the magnitude of the x-direction displacements of the corresponding nodal points combines the stiffness from the compression and tension sides and has proven to be able to prevent out-of-plane deformation at the end section. However, this coupling is only valid if symmetry about the horizontal diameter is maintained on the displaced end cross-section. The elastic boundary ring helps to maintain this symmetry.

3.3 *Applications of loads*

The pre- and post-buckling analyses of the shell segments have been carried out using the NISA program (Stegmüller, 1984). This program has been validated and used for a number of studies into shell behavior (see for instance Brendel and Ramm, 1980). Internal pressure is applied on the elements as an element load which is transformed into work equivalent nodal loads by the program. The external axial loads of equal magnitude and opposite direction are applied at the end cross-section and the mid-span cross-section. The axial load on the end section is uniformly distributed. The forces on the mid-span cross-section can be distributed in any manner because the axial displacements are coupled. The bending moment on the end section is applied as a set of nodal forces which are computed from a linear distribution. The elastic boundary ring helps to distribute the nodal loads and reduces stress concentrations which might cause initiation of premature buckling. Both internal pressure and axial load are maintained constant for a particular specimen but vary from specimen to specimen. The bending moments are determined by the equilibrium requirement after a certain overall curvature is imposed on the pipe segments in accordance with an arc-length solution technique (Zhou and Murray, 1995b).

3.4 *A brief note on the solution technique*

Shell structures may have severely nonlinear response due to large displacement effects and nonlinear material properties. For thin shell structures, development of local buckling leads to softening behavior in the postbuckling region. Softening behavior refers here to a characteristic of response in which moment carrying capacity decreases as the corresponding curvature increases. Prediction of response for this type of behavior is a challenge of numerical solution techniques.

A solution technique based on an equilibrium iterative procedure combined with an arc-length control technique has been used to carry out postbuckling analysis in this study. The procedure used is an arc-length method (see Schweizerhof and Wriggers, 1986), and is similar to that described by Bellini and Chulya (1987) but is considered to be an improvement over that presented in this latter paper. Details of this solution technique are discussed elsewhere by the authors (Zhou and Murray, 1995b).

4. POSTBUCKLING BEHAVIOR OF LINE PIPE

4.1 *Representation of deformations*

Nonlinear (postbuckling) analysis predicts the deformation, and the history of deformation, of the pipe segments. Computer renderings of typical configurations predicted by finite element analysis for post-buckled pipe segments are shown in Figs 4–9. Postbuckling behavior of these pipe segments with respect to the loading conditions is discussed subsequently, based on the analytical solutions for the 13 specimens listed in Table 1. However, in order to present the predicted response, two groups of representative quantities are

first defined. One is based on longitudinal deformations and the other on cross-sectional deformations.

Longitudinal deformations are described by *average curvatures* and *average strains* at the centroid of the cross-section in a similar way as for beam structures. That is, the relative rotations and relative shortening or extension of a specified segment are divided by the original length of the segment. Local deformations can be best represented by average curvature and strains defined on the buckling segment. These are referred to as the *local curvature*, ϕ_L, and the *local strain*, ε_L, respectively. The *buckling segment* is a small segment that is bounded by two plane sections and contains only the most significant buckle as shown in Fig. 3. The original length of the buckling segment is referred to as the *principal wavelength*. For comparison, average curvatures and strains are defined on the total pipe segment shown in Fig. 3 which results in the *overall curvature*, ϕ_O, and the *overall strain*, ε_O.

Three quantities are proposed to represent cross-sectional deformations. They are the *diametric differential*, D_d, *diametric expansion*, D_e, and *radius differential*, R_d. These are defined as

$$D_d = \frac{D_{out} - D_{in}}{D} \times 100\% \tag{1}$$

$$D_e = \left(\frac{D_{out} + D_{in}}{D} - 1\right) \times 100\% \tag{2}$$

$$R_d = \frac{R_{bot} - R_{top}}{R} \times 100\% \tag{3}$$

where D and R are the nominal diameter and radius of the pipe segment, respectively, and the other quantities are defined in Fig. 10. The measures D_{out} and D_{in} are the diameter in and out of the bending plane; and R_{bot} and R_{top} are the distances from the centroid of the cross-section to the extreme "tensile" fiber and "compressive" fiber in the bending plane, respectively, as shown in Fig. 10. The diametric differential is similar to the out-of-roundness, which is a commonly used measurement, and is defined as (see, for example, Price and Anderson, 1991)

$$\text{out-of-roundness} = \left(\frac{D_{max} - D_{min}}{D}\right) \times 100\% \tag{4}$$

where D_{max} and D_{min} are the maximum and minimum diameters of the cross-section, as shown in Fig. 10.

Diametric differential is intended for the deformation pattern in Fig. 10(a) where the dimension of the cross-section increases in the out-of-plane direction and decreases in the in-plane direction. It should be noted that the out-of-roundness is the absolute value of the diametric differential. While the former is commonly used in the oil and gas industry, the latter is the more informative because if differentiates between the two basic buckling modes. Diametric expansion is intended for the deformation pattern shown in Fig. 10(b) where the dimension of the cross-section increases in both the in-plane and out-of-plane directions. Radius differential represents components of cross-sectional deformations which are not symmetric about the y-axis. This measure would exclude ovalization and focus on deformations due to local buckling. It can be used as an indicator of initiation of local buckling.

4.2 *Moment–curvature relationships*

The moment–local curvature curves are shown in Figs 11–13 for specimens with low, middle and high levels of internal pressure, respectively. In these figures, the moments and local curvatures are normalized by the yield moment and yield curvature. The yield moment is the moment which, by itself, in the absence of internal pressure and axial force, produces initial yielding in the extreme fibers on both the compression and tension sides of the pipe

Fig. 4. Finite element prediction of deformed configuration for Specimen PLC40.

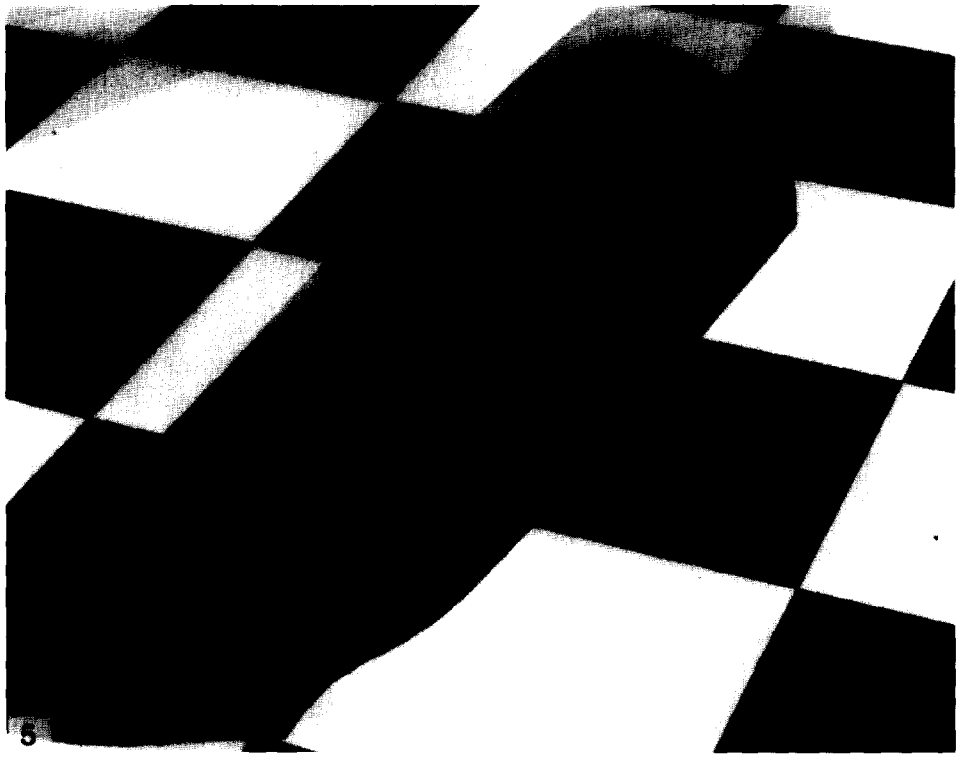

Fig. 5. Finite element prediction of deformed configuration for Specimen PLC00.

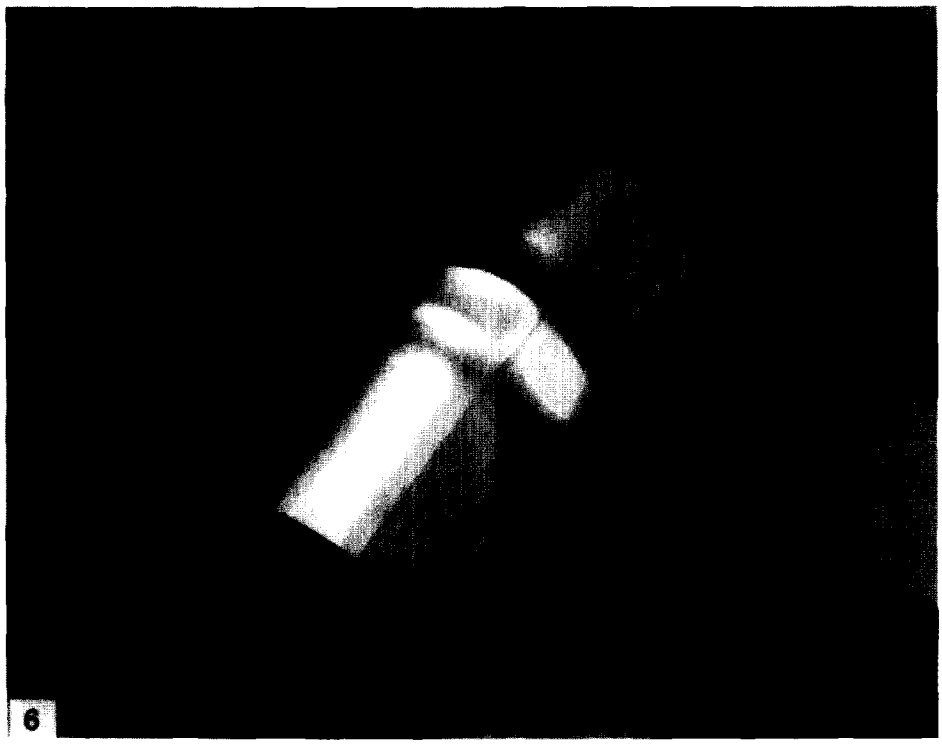

Fig. 6. Finite element prediction of deformed configuration for Specimen PMC40.

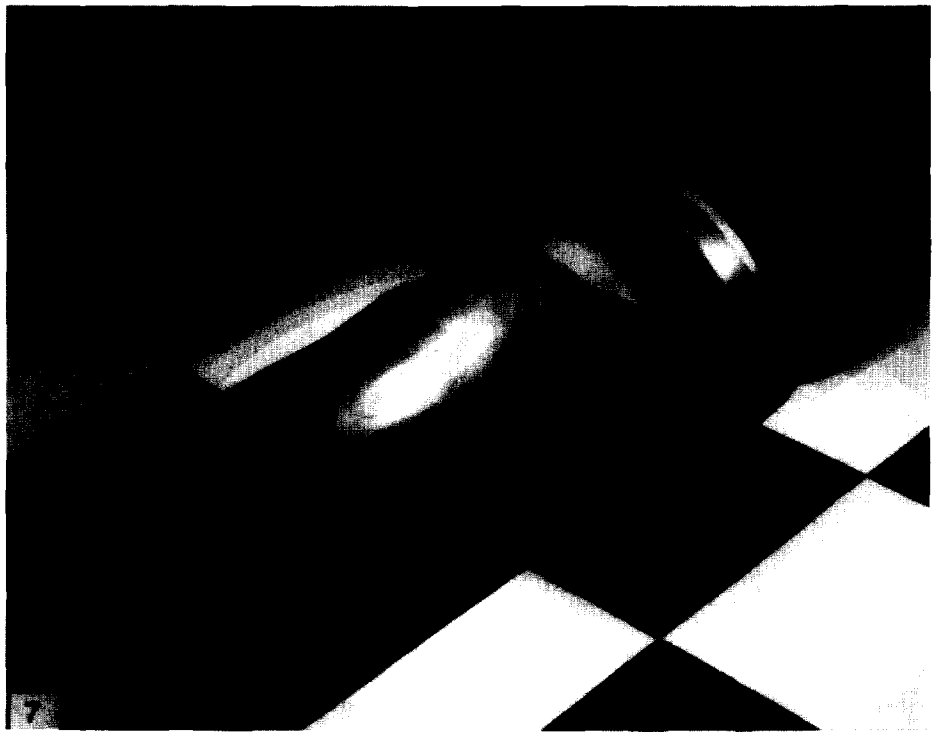

Fig. 7. Finite element prediction of deformed configuration for Specimen PHC40.

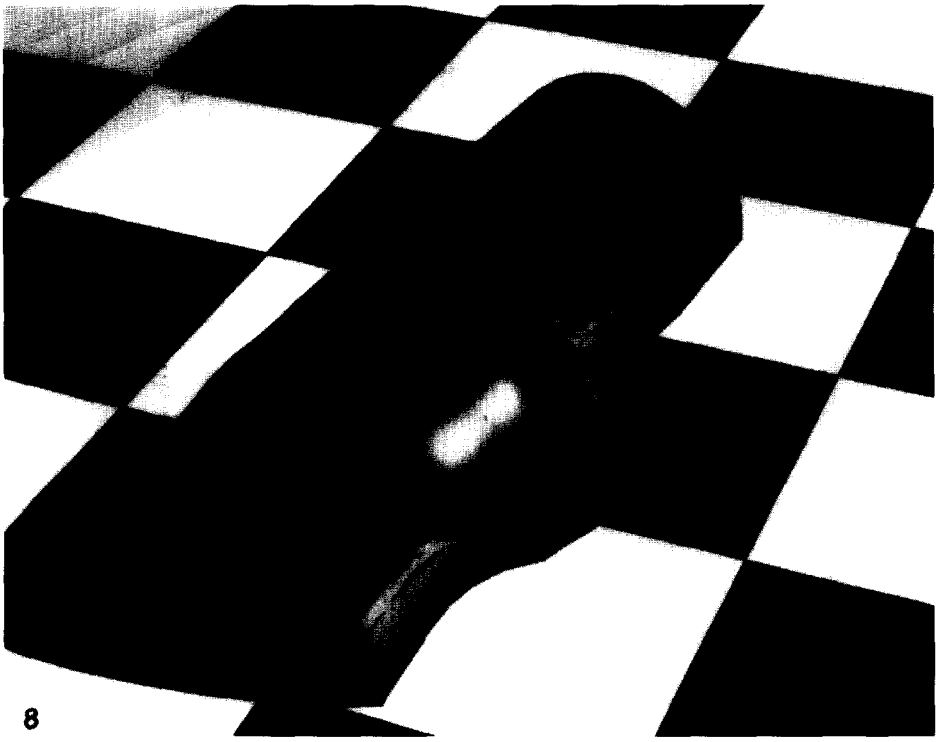

Fig. 8. Finite element prediction of deformed configuration for Specimen PHC00.

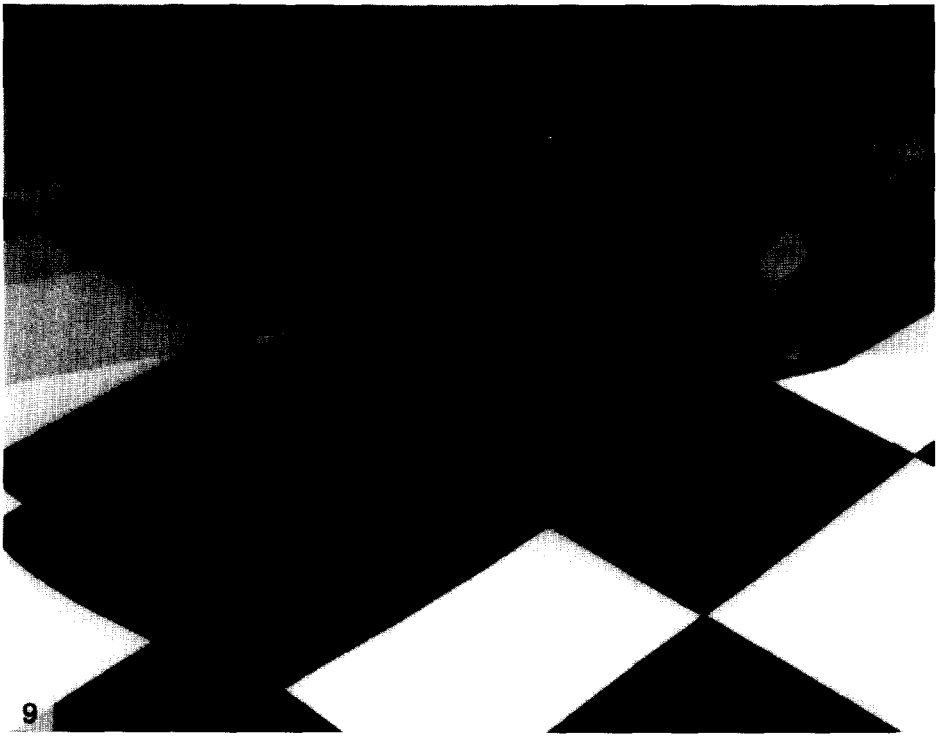

Fig. 9. Finite element prediction of deformed configuration for Specimen PHT40.

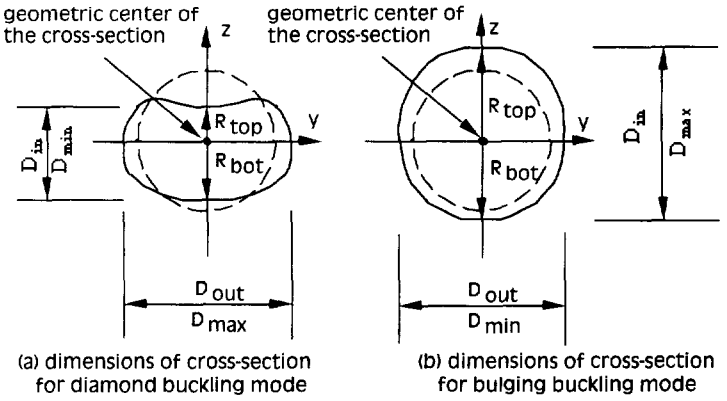

Fig. 10. Representative quantities of cross-sectional deformations for postbuckling.

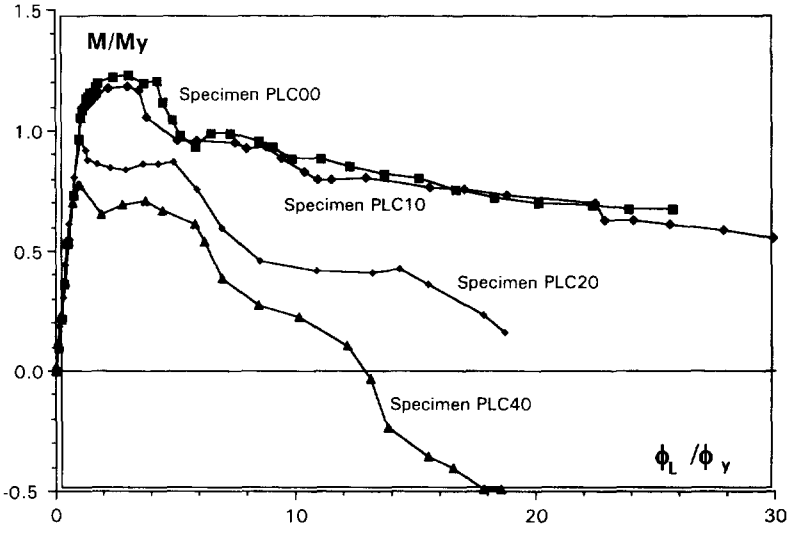

Fig. 11. Moment–local curvature curves for specimens with low level pressure.

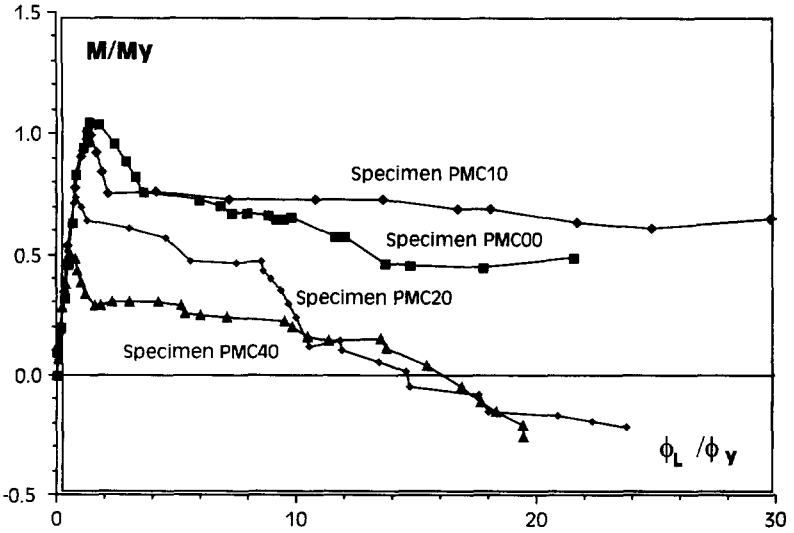

Fig. 12. Moment–local curvature curves for specimens with middle level pressure.

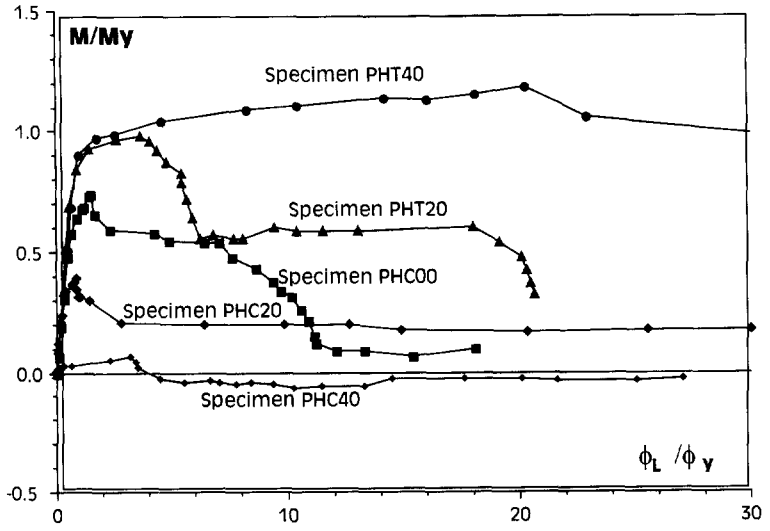

Fig. 13. Moment–local curvature curves for specimens with high level pressure.

for the bilinear elastic–plastic model. This is calculated to be 52000 kip-in (5900 KN m). The yield curvature is the curvature corresponding to the yield moment. It is calculated as 0.8965×10^{-4}/in (0.353×10^{5}/mm).

In general, the pipe segment experiences a linear elastic region up to the initiation of yielding, a gradual yielding region, and then a softening region (see, for example, Specimens PLC00 and PLC10 in Fig. 11). The elastic region exists in every specimen except Specimen PHC40 (see Figs 11–13) where the constant internal pressure and axial load initiate the yielding before any moment is applied. The gradual yielding region produces a yield plateau which usually contains the limit point for the maximum moment as for Specimens PLC00, PLC10, PHT20 and PHT40. The length of this yield plateau decreases as the levels of pressure and compressive axial load increase and virtually disappears for many specimens. The softening region exists in every moment-curvature curve. Softening in moment-curvature curves refers to behavior which exhibits decreasing moment-carrying capacity with respect to increasing curvature.

The maximum moment carried by specimens is greatly affected by the pressure and axial load. It varies from a maximum of 1.23 times the yield moment for Specimen PLC00, where no pressure and axial load are applied, to 0.11 times the yield moment for Specimen PHC40, where the maximum pressure and compressive axial load are applied. The capacity in the postbuckling region is affected by pressure and axial loading in a similar way as for the maximum capacity. The effects of axial load are illustrated in Figs 11–13 at different levels of pressure. In a similar way, the effects of pressure are illustrated for constant axial force in Fig. 14, where solutions with zero axial load are shown.

As pipe segments soften in the postbuckling region, deformations localize into a dominant 'wrinkle' in the buckling segment (see, for instance, Mohareb *et al.*, 1993). While the buckling segment continues to be loaded (in the sense that deformations continue to increase), the rest of the pipe segment unloads elastically. Energy released from elastic unloading further increases localization of deformation in the buckling segment. Figures 15–17 show the axial strain–curvature curves, which are referred to as deformation paths, for specimens PLC00, PLC40 and PHC40. Deformation paths for the buckling segment and for the pipe segment as a whole are referred to as the local and overall deformation paths, respectively. The localization of deformation is clearly demonstrated in all these figures where the local curvature and axial strain are significantly larger than the overall curvature and axial strain. For specimens such as PLC00, the localization is essentially associated with flexural deformation. This is indicated by the large difference in curvatures and relatively small difference in axial strains shown in Fig. 15. The contribution of axial deformation to localization becomes more important as the pressure and compressive axial load increase. This is illustrated by Figs 16 and 17. The solutions of the 13 specimens

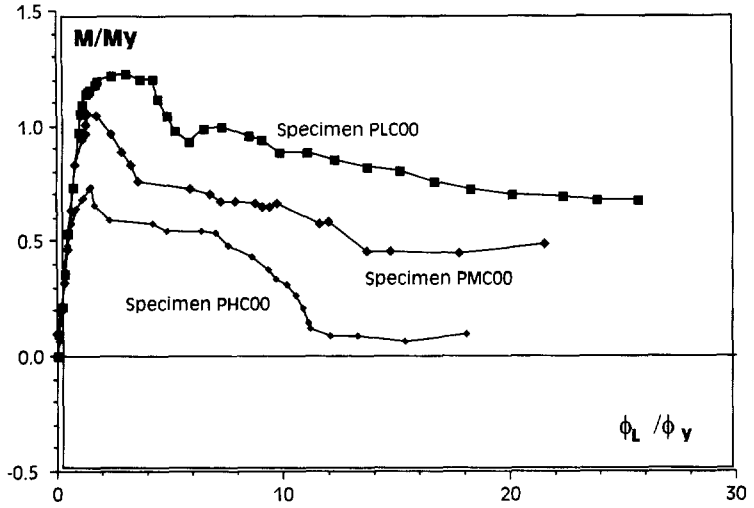

Fig. 14. Moment–local curvature curves for specimens without axial load.

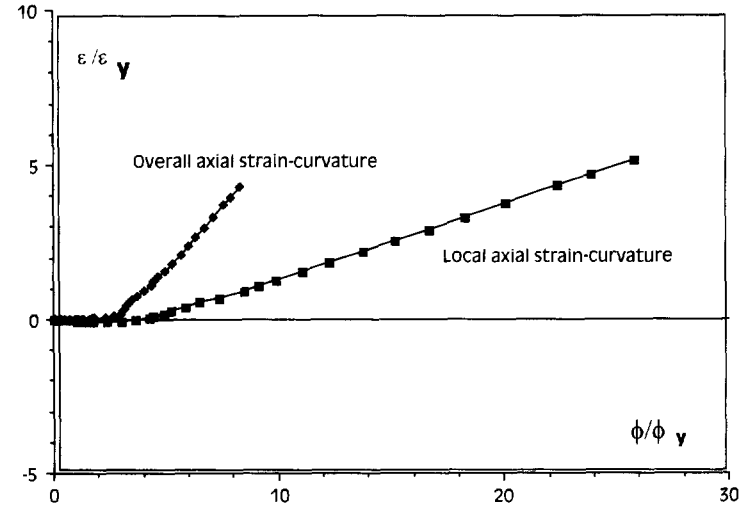

Fig. 15. Deformation paths of Specimen PLC00.

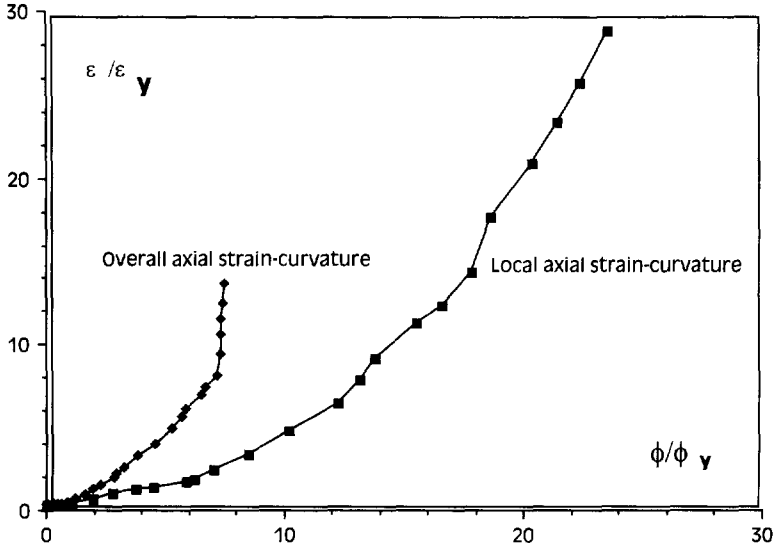

Fig. 16. Deformation paths of Specimen PLC40.

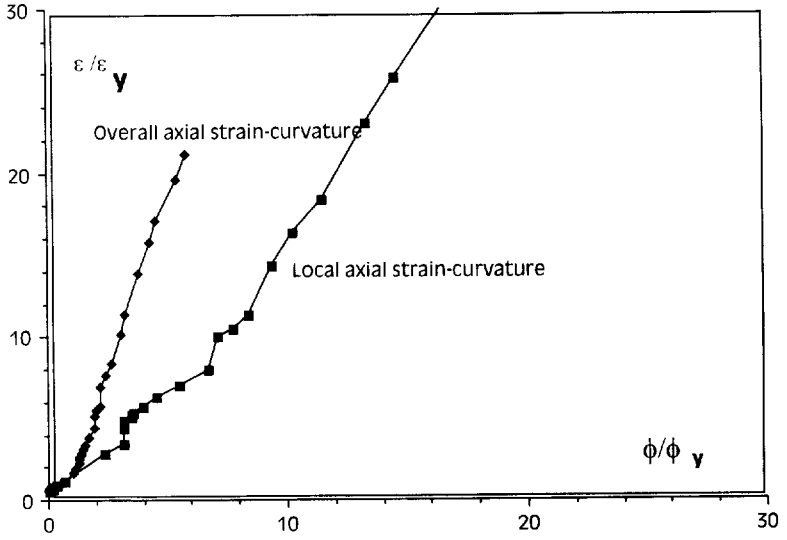

Fig. 17. Deformation paths of Specimen PHC40.

indicate that internal pressure and compressive axial load increase the localization of deformation.

4.3 *Buckling modes*

Local buckling deformations have been predicted to large amplitudes, as is shown in Figs 4–9 which are true scale renderings of finite element results. (Note that the linear dimension of the squares depicted on the loading plane is equal to the undeformed diameter of the pipe.) The buckling configurations can be grouped into two types of modes based on their common characteristics. These are denoted as *diamond modes* and *bulging modes*. A typical diamond mode is shown in Fig. 4 where the buckle consists of several dips in a regular pattern. The dips have a diamond shape and the pipe wall in the dips moves toward the centroid of the cross-section. The mode shown in Fig. 5 is sometimes referred to as the Brazier mode (Timoshenko and Gere, 1961). However, it is classified here as a diamond mode since it can be viewed as a special case with only one large dip. A typical bulging mode is shown in Fig. 6 where a bulge is developed and the pipe wall in the bulge moves outward. The buckling modes shown in Figs 6–9 have this common characteristic and therefore all are classified as bulging modes. The multiple wrinkles in Fig. 7 are formed by continuing the analysis beyond the softening range associated with the first wrinkle until a second wrinkle forms in a manner similar to the first.

It is clear that an entire spectrum of buckling configurations can occur. It is also clear that the type of buckling mode is primarily dependent on the internal pressure. Specimens without pressure buckle in diamond modes no matter what axial load is applied. However, specimens with middle and high levels of pressure buckle in bulging modes. The results show that, for the geometric and material properties used in this study, internal pressure at a relatively low level, certainly not higher than $0.35\,p_y$, can prevent the pipe segment from buckling in the diamond buckling mode and force it to buckle in a bulging buckling mode. This conclusion is likely to extend to pipe segments with D/t ratios lower than 104, since shells with higher D/t ratios have a greater tendency to buckle in diamond modes.

The effects of axial load on buckling modes are also illustrated in Figs 4–9. In addition to the differences between the diamond and bulging buckling modes, obvious differences exist between the buckling modes of Specimens PLC00 and PLC40 for the diamond buckling modes, and between Specimens PHT40 and PHC40 for the bulging buckling modes. The principal difference is in the extent of the buckles in the circumferential direction. The buckles of Specimens PLC00 and PHT40 are confined to the compressive side of the pipe segment. The buckles of Specimens PLC40 and PMC40, however, cover most of, or the entire, circumference. This is because of the different combinations of the

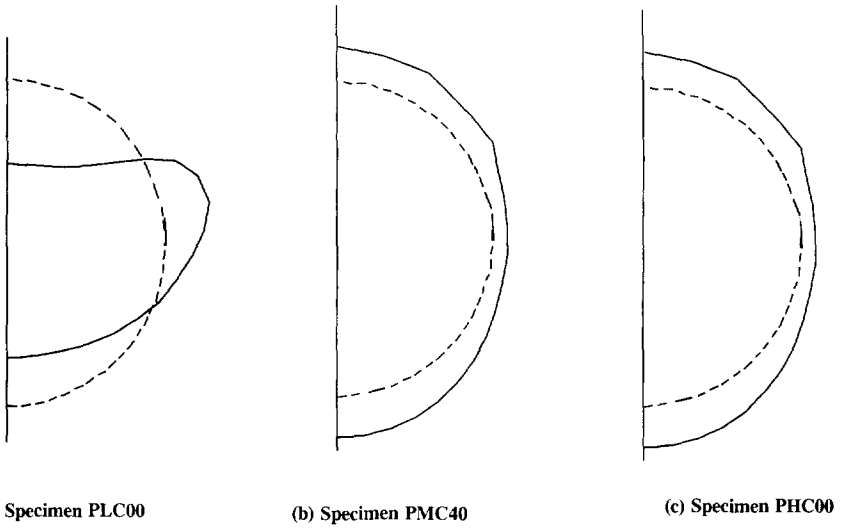

(a) Specimen PLC00 (b) Specimen PMC40 (c) Specimen PHC00

Fig. 18. Cross-sectional distortion for Specimens PLC00, PMC40, and PHC00.

axial deformation and flexural deformation. When the flexural deformation dominates, the compressive region on the cross-section is confined to the compressive side and so is the buckle, as shown in Figs 5, 8 and 9. When significant compressive axial load is applied, as for Specimens PLC40, PMC40 and PHC40, the compressive region extends over most of the cross-section and buckles develop gradually to cover most of the circumference. Tensile axial loads help to confine the buckle to the compressive side of the cross-section. To distinguish between these two different characteristics, the designations of *flexural deformation dominated* and *axial deformation dominated* buckling modes are used to distinguish between buckling modes confined to the compressive side and extended over most of the circumference, respectively. Both diamond and bulging buckling modes can be dominated by flexural or axial deformation. The compressive axial load and internal pressure both accentuate the axial deformation and lead to axial deformation dominated buckling modes.

4.4 *Cross-sectional deformations*

Cross-sectional deformation becomes important because its measurement permits the establishment of criteria by which limit states of excessive deformation can be defined. Depending on the buckling mode, different patterns of cross-sectional deformation are observed. Typical examples are shown in Fig. 18 for Specimens PLC00, PMC40, and PHC00. For each of the deformed cross-sections, there is a reference section, shown by the dashed line, which has the centroid at the same location as for the deformed section but is undeformed. The scale of deformation is one to one of all the deformed cross-sections and the figures show the real proportions of the deformation.

Specimen PLC00 is a typical example of a flexural deformation dominated diamond buckling mode. For this type of buckling mode, the diameter in the bending plane, called the in-plane diameter, is significantly reduced while the diameter perpendicular to the bending plane, called the out-of-plane diameter, is increased. An appropriate measurement of the magnitude of cross-sectional distortion for this type of buckling mode is the diametric differential defined in eqn (1) which is the normalized differential between the out-of-plane and in-plane diameters. The cross-sectional deformation develops from being negligible at the onset of buckling to being very significant in the deep postbuckling region. The diametric differential–curvature curve for Specimen PLC00, along with those for other specimens with low pressure level, is shown in Fig. 19.

Examples for the bulging type buckling modes are shown in Figs 18(b) and 18(c), for Specimens PMC40 and PHC00, respectively, where the former is an axial deformation dominated bulging buckling mode and the latter is a flexural deformation dominated bulging mode. For bulging type buckling modes, both in-plane and out-of-plane diameters

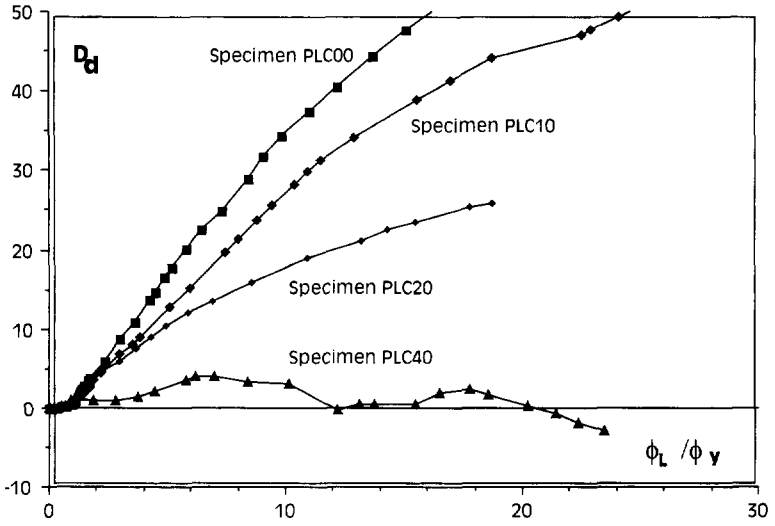

Fig. 19. Diametric differential for specimens with low level pressure.

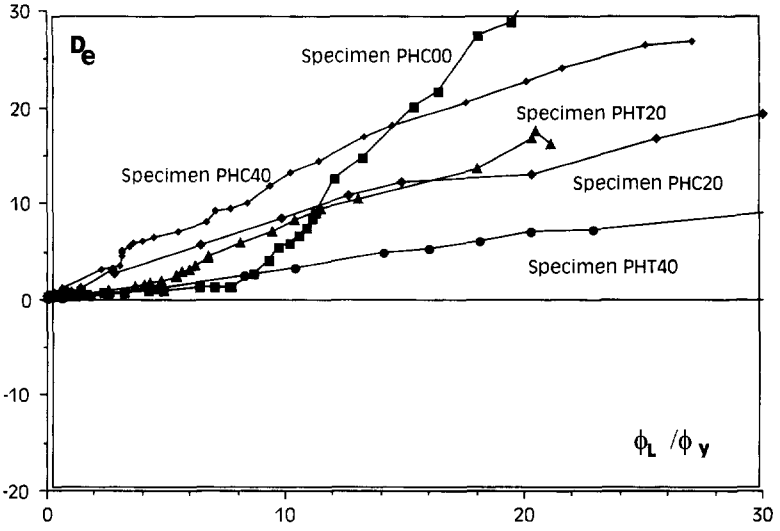

Fig. 20. Diametric expansion for specimens with high level pressure.

increase as the curvature increases. When the buckling is dominated by axial deformation, the increase in diameter is more uniform along the circumference, as in Fig. 18(b) which is typical of axially symmetric buckling modes. When the flexural deformation dominates, the increase of in-plane diameter is larger than that of the out-of-plane diameter as shown in Fig. 18(c). One of the representative measurements for the magnitude of cross-sectional deformation for bulging type buckling modes is the diametric expansion defined in eqn (2) which is the normalized average increase of in-plane and out-of-plane diameters. Diametric expansion–curvature curves for specimens with high level pressures are shown in Fig. 20.

5. STIFFNESS CHARACTERISTICS REPRESENTED BY STIFFNESS-PROPERTY DEFORMATION RELATIONS

One of the objectives of postbuckling analysis is to define and generate characteristic stiffness properties of the pipeline segment throughout its deformation history. These stiffness properties may then be input into an analysis of the pipeline based on a beam model. As a result, the local behavior, dominated by local buckling, is integrated into the overall response of the pipeline. A primary objective of this paper is to discuss a process by which the stiffness properties may be determined. We now focus on the definition of

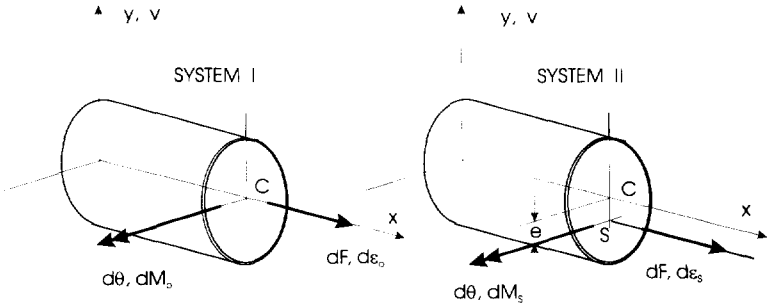

Fig. 21. Reference systems for stress resultants and deformation coordinates.

stiffness properties, the *stiffness-property–deformation* (SPD) relations and the procedures to generate and apply SPD relations.

In the derivations, the subscript "c" will refer to quantities at the centroidal axis of the cross-section at the end supports of the segment shown in Figs 1 and 3. The subscript "o" will refer to quantities at a longitudinal axis through the centroid of the cross-section at an arbitrary position along the length, and the subscript "s" will refer to quantities at a longitudinal axis through the centroid of the transformed section at an arbitrary position along the length, as illustrated in Fig. 21. Quantities which are the same for both the "s" and "o" axes are not subscripted.

5.1 *Definition of cross-sectional stiffness coefficients*

Assuming that the stress resultants F and M_o are single valued integrable functions of the generalized displacements ϕ and ε_o the increments of stress resultants may be expressed by the chain rule as

$$\mathrm{d}^t F = \frac{\partial^t F}{\partial^t \varepsilon_o}\mathrm{d}^t \varepsilon_o + \frac{\partial^t F}{\partial^t \phi}\mathrm{d}^t \phi \tag{5a}$$

$$\mathrm{d}^t M_o = \frac{\partial^t M_o}{\partial^t \varepsilon_o}\mathrm{d}^t \varepsilon_o + \frac{\partial^t M_o}{\partial^t \phi}\mathrm{d}^t \phi \tag{5b}$$

in which the partial derivatives are the incremental stiffness coefficients and the pre-superscript t refers to the structural configuration at time t, consistent with the incremental notation of Bathe (1982). Using a change in notation these equations may be written as

$$\mathrm{d}^t F = K_1\,\mathrm{d}^t \varepsilon_o + K_3\,\mathrm{d}^t \phi \tag{6a}$$

$$\mathrm{d}^t M_o = K_3\,\mathrm{d}^t \varepsilon_o + K_2\,\mathrm{d}^t \phi \tag{6b}$$

where the stiffness coefficients in eqns (6) are defined by identifying corresponding terms between eqns (5) and (6) and it has been assumed that the stiffness coefficients in eqns (6) are symmetric. This is proved in Appendix A, where it is shown that

$$K_3 = \frac{\partial^t F}{\partial^t \phi} = \frac{\partial^t M_o}{\partial^t \varepsilon_o} = eK_1 \tag{7}$$

in which e is the eccentricity between the center of elastic stiffness and the center of the tangent modulus stiffness, as shown in Fig. 21. For brevity these two centers of stiffness are referred to as the *centroid* and the *tangent centroid*, respectively.

It is necessary to evaluate the stiffness coefficients K_1 and K_2, and the eccentricity, e, in order to integrate eqns (6) numerically. This is not as straightforward as it may appear because these coefficients must be derived numerically from the shell solutions for the segments, and the incremental stiffnesses which are directly available from the segment solutions do not correspond with those appearing in eqns (6). By definition, the coefficients in eqns (5) and (6) are partial derivatives with respect to each of the generalized displacements while the other generalized displacement is being held constant. The constraint

condition on the second generalized displacement, while the first is incremented is not satisfied in the segment solutions. Therefore, we define another set of quantities in the following, related to the segment solutions. We will then show how the stiffness coefficients of eqns (6) are derivable from this second set.

5.2 *Stiffness properties derivable from segment solutions*

The shell model of a pipe segment that is used to determine the pipe stiffness has been shown in Fig. 1. The reference axis is taken to be the centroidal axis. A solution path for an equilibrium solution is traced by maintaining F_c constant and incrementing M_c. When a small increment of M_c is applied, the pipe deforms along its total length. The region of greatest interest is the region where the wrinkle is developing, as shown in Fig. 3, and for which the analyst wishes to construct relations such as moment–curvature curves. We define a number of response characteristics, that are associated with the loading, which we will call *stiffness properties*.

(1) *Property* 1: *flexural stiffness*, ${}^{t}K_b$ The flexural stiffness is evaluated by applying an increment in moment, ΔM_c, while holding the axial force constant. It is defined at the location of the wrinkle as

$$ {}^{t}K_b = \frac{\partial\, {}^{t}M_o}{\partial\, {}^{t}\phi} \quad \text{with } {}^{t}F = \text{constant}. \tag{8} $$

This stiffness property is simply the slope of one of the moment–curvature curves, as plotted in Figs 11–15. However, the reader should note that the constraint part of this equation, which appears behind the relational part, is as important as the relational part. [This statement is also true for subsequent equations, such as eqn (9).]

In addition, it is apparent that $M_o \neq M_c$ and, therefore, the determination of the moment–curvature curve from the incremental analysis requires considerable processing of the numerical results produced by the incremental analysis of the specimen (see Section 5.3).

(2) *Property* 2: *axial stiffness*, ${}^{t}K_a$. The axial stiffness is evaluated by applying an increment of axial force, ΔF_c, to the ends of the segment shown in Fig. 1, while keeping $\Delta M_c = 0$. It is defined as

$$ {}^{t}K_a = \frac{\partial\, {}^{t}F}{\partial\, {}^{t}\varepsilon_o} \quad \text{with } \mathrm{d}\, {}^{t}M_o = {}^{t}C\, {}^{t}r_o\, \mathrm{d}\, {}^{t}F_c. \tag{9} $$

The constraint part of this equation arises from the fact that the moment along the length changes as a result of the eccentricity, ${}^{t}r_o$, even though $\Delta M_c = 0$.

(3) *Property* 3: *the amplification factor*, ${}^{t}C$. For the loading associated with Property 2 the increase of moment at the centroid at the location of the wrinkle may be expressed, by statics, as

$$ \mathrm{d}\, {}^{t}M_o = \mathrm{d}\, {}^{t}M_c + {}^{t}F_c\, \mathrm{d}\, {}^{t}r_o + {}^{t}r_o\, \mathrm{d}\, {}^{t}F_c. \tag{10} $$

Since the first term on the right-hand side of eqn (10) is zero, factoring the last term yields the constraint in eqn (9), and leads to the definition of the amplification factor, ${}^{t}C$, as

$$ {}^{t}C = 1 + \frac{{}^{t}F_c\, \mathrm{d}\, {}^{t}r_o}{{}^{t}r_o\, \mathrm{d}\, {}^{t}F_c}. \tag{11} $$

Knowing ${}^{t}C$ the change in moment at the wrinkle can be evaluated by the constraint relationship in eqn (9) whenever a change in end force occurs.

(4) *Property* 4: *location of centroid*, ${}^{t}v_o$. The location of the centroid of the cross section relative to its original configuration can be expressed as

$$ {}^{t}v_{o} = \frac{\int_{A} {}^{t}v \, \mathrm{d}A}{\int_{A} \mathrm{d}A} \tag{12} $$

where ${}^{t}v$ is the displacement in the global z-direction as shown in Fig. 1.

(5) *Property* 5: *location of tangent centroid*, ${}^{t}y_{o}$. The location of the tangent centroid of the cross section (note that this term has been defined above) can be expressed as

$$ {}^{t}y_{o} = \frac{\int_{A} {}^{t}E \, {}^{t}y \, \mathrm{d}A}{\int_{A} {}^{t}E \, \mathrm{d}A} \tag{13} $$

where ${}^{t}E$ is the tangent modulus (for the proper sense of $\Delta\varepsilon$) and ${}^{t}y$ is the coordinate of the point measured in the y direction of Fig. 21 (which is the global z-direction of Fig. 1). Note that the coordinate system of Fig. 21 is being used because it is consistent with a normal two-dimensional beam model whereas the coordinate system in Fig. 1 is for the shell analysis.

The five properties above are collectively defined as the stiffness-properties of the pipe, all of which are dependent on the deformations of the pipe. These properties may be determined from the configuration of the three-dimensional shell, according to their definitions above, at any stage of deformation on the path of an equilibrium solution. The result is to produce a set of *stiffness-property–deformation* relationships (i.e. SPD relations). For convenience in producing SPD relations, SPD relations are defined herein in the form of Stiffness-Property–Local-Curvature relations at specified constant levels of axial load. The procedure to generate a set of SPD relations is discussed in Section 5.3.

5.3 *Generation of SPD relations*

Three-dimensional shell analyses of a pipeline segment, as described in Section 3, are needed to generate SPD relations. The average response in the buckled segment is used to construct the SPD relations. In principle the buckled segment could be located anywhere on the pipeline segment, as indicated in Fig. 3, although it is more likely to be located in the central part than at the ends. The geometric and material properties for the shell model are the same as those of the pipeline to be analyzed in the beam model.

Two types of run of the shell analysis, which can be called the *primary run* and *secondary runs*, respectively, are necessary to define the five SPD relations at each of the specified axial loads. The primary runs starts from the initial state and proceeds incrementally at proper step-sizes under constant axial load, constant internal pressure and incremental bending moment. The primary run is stopped when the deformation of the pipeline becomes large enough so that the pipeline is obviously no longer operational. The secondary runs start from any equilibrium state on the path of the primary run, and consist of a one-step incremental solution of relatively small step-size under constant applied moment, constant internal pressure and incremental axial load. The secondary runs may be initiated from restart files generated during the primary run, after the primary run is completed. They are stopped after one step.

The primary run provides the information to construct three SPD relations at the specified axial force. These are: the moment–curvature relation which defines the flexural stiffness, ${}^{t}K_{b}$ of eqn (8); the ${}^{t}v_{o}$-curvature relation defining the location of the centroid by eqn (12); and the ${}^{t}y_{o}$-curvature relation defining the location of the tangent centroid, as given by eqn (13). The moment–curvature relation comes naturally out of the primary run where moment and curvature are defined as the average values on the buckled segment. The location of the centroid, ${}^{t}v_{o}$, and the tangent centroid, ${}^{t}y_{o}$, are obtained by integration

over the cross-section. The integration should be carried out over several cross-sections and their average is used to define SPD relations for the buckled segment.

The series of secondary runs along the path of the primary run at proper intervals provides the information to construct two SPD relations at the specified axial force. These are the axial stiffness (i.e.-$'K_a$)-curvature relation defining the axial stiffness of eqn (9), and the $'C$-curvature relation defining the amplification factor of eqn (11). The axial stiffness $'K_a$ can be obtained according to the definition because the constraint in eqn (9) is satisfied in the secondary run. The amplification factor can be evaluated since the increments of $'F$ and $'v_o$ are available from the solutions of the secondary runs.

5.4 *Application of SPD relations*

With the SPD relations established, the stiffness coefficients of eqns (6) and (7) can be expressed in terms of the stiffness properties as follows. First, the eccentricity e of Fig. 21, as required for the evaluation of K_3 in eqn (7), may be determined from the positions of the centroids as

$$e = 'y_o - 'v_o. \tag{14}$$

Next, eqn (6) can be used to express the conditions associated with Property 1. The constraint part of eqn (9) can be expressed using eqn (6a) as

$$0 = K_1 \, d\varepsilon_o + eK_1 \, d\phi \tag{15}$$

from which

$$d\varepsilon_o = -e \, d\phi. \tag{16}$$

Substituting eqn (16) into eqn (6b) and factoring $d\phi$

$$dM_o = (K_2 - e^2 K_1) \, d\phi. \tag{17}$$

Dividing by $d\phi$, and recognizing that the result corresponds to the definition of eqn (8) we have

$$'K_b = \frac{\partial \, 'M_o}{\partial \, '\phi} = K_2 - e^2 K_1. \tag{18}$$

Next, eqns (6) are used to express the conditions associated with the definition of Property 2. The constraint part of eqn (9) can be expressed by eqn (6b) as

$$'C \, 'v_o \, d'F = e \, 'K_1 \, d'\varepsilon_o + 'K_2 \, d'\phi. \tag{19}$$

Solving for $d'\phi$ yields

$$d'\phi = \frac{'C \, 'v_o \, d'F - e \, 'K_1 \, d'\varepsilon_o}{'K_2}. \tag{20}$$

Substituting this into eqn (6a), grouping terms and factoring $d'F$ and $d'\varepsilon_0$, results in

$$\frac{d'F}{d'\varepsilon_o} = \frac{'K_1 \, 'K_2 - e^2 \, 'K_1^2}{'K_2 - e \, 'C \, 'v_o \, 'K_1} = 'K_a \tag{21}$$

where the latter equality arises from a recognition that the left hand side is the quantity defined in eqn (9) for Property 2.

Equations (18) and (21) can be solved simultaneously for the stiffness coefficients K_1 and K_2, to yield

$$'K_1 = \frac{'K_a \, 'K_b}{'K_b - e^2 \, 'K_a + e \, 'C \, 'v_o \, 'K_a} \tag{22}$$

and

$$ {}^{t}K_2 = \frac{{}^{t}K_b^2 + e^{t}C^{t}v_o\,{}^{t}K_a\,{}^{t}K_b}{{}^{t}K_b - e^{2}{}^{t}K_a + e^{t}C^{t}v_o\,{}^{t}K_a}. \tag{23} $$

Each of the stiffness coefficients in eqns (22) and (23) is dependent on all five stiffness-property–deformation quantities. When these are known, the behavior of the pipeline-beam can be predicted by the direct stiffness technique, including the effects of plastic deformation and local buckling, by integrating eqns (6). The technique for carrying out the beam analysis, and the verification that the integration of eqns (6) yields acceptable results when the stiffness coefficients have been determined in the above manner, is addressed in Zhou and Murray (1993a, 1995a).

6. CONCLUSIONS

The paper has described a three-dimensional shell model for postbuckling analysis of pipeline segments. Solutions are obtained for a particular pipe subjected to several loading conditions and are presented in terms of both longitudinal and cross-sectional measures of deformation as proposed herein.

Postbuckling behavior is discussed with respect to the characteristics of moment–curvature curves, buckling modes and cross-sectional deformations. Both internal pressure and axial load are found to have significant influence on the postbuckling behavior.

To integrate effects of local shell buckling into overall response of pipelines, a set of stiffness properties are defined in terms of SPD relations with respect to the deformation path. A procedure to generate SPD relations is described. The stiffness coefficients to evaluate the stiffness of the pipeline as a beam, including the effects of local shell buckling, are then expressed in terms of the stiffness properties.

Acknowledgements—The research upon which this paper is based was carried out by the junior author in partial fulfillment of the requirements for the degree of Doctor of Philosophy in Civil Engineering, at the University of Alberta. The authors wish to express their appreciation to the Center for Frontier Engineering Research (C-Fer), and to the Faculty of Graduate Studies of the University of Alberta, for their financial support of this project.

REFERENCES

Bathe, K-J. (1982). *Finite Element Procedures in Engineering Analysis*. Prentice-Hall, Inc., Englewood Cliffs, New Jersey.

Bellini, P. X. and Chulya, A. (1987). An improved automatic incremental algorithm for the efficient solution of nonlinear finite element equations. *Comput. Struct.* **26**(12), 99–110.

Bouwkamp, J. G. and Stephen, R. M. (1973). Large diameter pipe under combined loading. *Transportation Journal of the ASCE*. **99**(TE3), 521–536.

Brendel, B. and Ramm, E. (1980). Linear and nonlinear stability analysis of cylindrical shells. *Comput. Struct.* **12,** 549–558.

Canadian Standards Association (1990). CAN/CSA-Z183-M90 Oil Pipeline Systems.

Jirsa, J. O., Lee, F. H., Wilhoit, J. C. and Merwin, J. E. (1972). Ovaling of pipelines under pure bending. Offshore Technology Conference, Paper No. OTC 1569.

Mohareb, M., Alexander, S. D. B., Kulak, G. L. and Murray, D. W. (1993). Laboratory testing of line pipe to determine deformational behavior. In *Proc. of the 12th Int'l Conf. on OMAE* (Edited by S. K. Chakrabarti, C. Aage, H. Maeda, A. N. Williams and D. Morrison), Vol. V-Pipeline Technology, pp. 109–114. ASME, Glasgow.

Price, P. St. J. and Anderson, H. A. (1991). Integrity monitoring and maintenance criteria for new and existing on land and marine pipelines. In *Proceeding of the First International Offshore and Polar Engineering Conference* (Edited by M. S. Triantafyllou, K. Karal, Jin S. Chung, G. C. Hartnup and S. S. Gowda), Vol. 11, pp. 386–393. Edinburgh, United Kingdom.

Reddy, B. D. (1979). An experimental study of the plastic buckling of circular cylinders in pure bending. *Int. J. Solids Structures*. **15,** 669–683.

Schweizerhof, K. and Wriggers, P. (1986). Consistent linearization for path following methods in nonlinear FE analysis. *Comput. Meth. Appl. Mech. Engng* Elsevier Science Publishers (North Holland) **59,** 261–279.

Sherman, D. R. (1976). Tests of Circular Steel Tubes in Bending. *J. Struct. Div. ASCE*. **102**(ST11), 2181–2195.

Stegmüller, H. (1984). *Nonlinear Inelastic Structural Analysis (NISA)–The User Manual*. Institut Fur Baustatik, Univeritat Stuttgart, Stuttgart, West Germany.

Timoshenko, S. and Gere, J. M. (1961). *Theory of Elastic Stability, second edition*. McGraw-Hill Book Company Inc., New York.

Zhou, Z. and Murray, D. W. (1993a). Numerical structural analysis of buried pipelines. Structural Engineering Report 181. Dept. of Civil Engineering, Univ. of Alberta, Edmonton AB, Canada T6G 2G7.

Zhou, Z. and Murray, D. W. (1993b). Behavior of buried pipelines subjected to imposed deformations. In *Proc. of the 12th Int'l Conf. on OMAE* (Edited by S. K. Chakrabarti, C. Aage, H. Maeda, A. N. Williams and D. Morrison), Vol. V-Pipeline Technology, pp. 115–122, ASME, Glasgow.

Zhou, Z. and Murray, D. W. (1993c). Towards rational deformation limit states for buried pipelines. In *Proc. of the 3rd ISOPE Conf.* (Edited by J. S. Chung, K. Karal, M. S. Triantafyllou and R. W. Fredenking), Vol II, pp. 18–24.

Zhou, Z. and Murray, D. W. (1995a). Formulation and verification for pipeline beam models using stiffness-property–deformation relations. *J. of Transportation Engng, ASCE* (in press).

Zhou, Z. and Murray, D. W. (1995b). An incremental solution technique for unstable equilibrium paths of shell structures. *Comput. Struct.* (in press).

APPENDIX

Derivation of equation (7)

Assume an instantaneous center of stiffness (equivalent to the centroid of a transformed section for the tangent modulus E values) exists, and is located at a point s at a distance of e from the centroid, c, of the cross section, as shown in Fig. 21. The generalized stiffness relations are then uncoupled with respect to the s axis and we may write, for an element of unit length,

$$\begin{Bmatrix} \mathrm{d}F \\ \mathrm{d}M_s \end{Bmatrix} = \begin{bmatrix} K_1 & 0 \\ 0 & \tilde{K} \end{bmatrix} \begin{Bmatrix} \mathrm{d}\varepsilon_s \\ \mathrm{d}\phi \end{Bmatrix} = \mathbf{K}_s \begin{Bmatrix} \mathrm{d}\varepsilon_s \\ \mathrm{d}\phi \end{Bmatrix}. \tag{A1}$$

For plane sections the geometry relating the generalized displacements between the two axes is

$$\begin{Bmatrix} \mathrm{d}\varepsilon_s \\ \mathrm{d}\phi \end{Bmatrix} = \begin{bmatrix} 1 & e \\ 0 & 1 \end{bmatrix} \begin{Bmatrix} \mathrm{d}\varepsilon_o \\ \mathrm{d}\phi \end{Bmatrix} = \mathbf{T} \begin{Bmatrix} \mathrm{d}\varepsilon_o \\ \mathrm{d}\phi \end{Bmatrix} \tag{A2}$$

in which $\mathbf{T}$ is the geometric transformation matrix and it is recognized that ϕ is the same for each system of displacements. By the theorem of contragredience, the force transformation matrix is $\mathbf{T}^{\mathrm{T}}$, and the stiffness relationship between the forces and displacements referenced to the centroidal axis is

$$\begin{Bmatrix} \mathrm{d}F \\ \mathrm{d}M_o \end{Bmatrix} = \mathbf{T}^{\mathrm{T}} \mathbf{K}_s \mathbf{T} \begin{Bmatrix} \mathrm{d}\varepsilon_o \\ \mathrm{d}\phi \end{Bmatrix} = \mathbf{K}_o \begin{Bmatrix} \mathrm{d}\varepsilon_o \\ \mathrm{d}\phi \end{Bmatrix} \tag{A3}$$

where $\mathbf{K}_o$ represents the matrix product and may be expressed as

$$\mathbf{K}_o = \begin{bmatrix} K_1 & eK_1 \\ eK_1 & K_2 \end{bmatrix} \tag{A4}$$

with K_2 being defined as

$$K_2 = \tilde{K} + e^2 K_1. \tag{A5}$$

When compared to eqns (5) and (6), eqns (A3) and (A4) establish the validity of eqn (7).